Published in final edited form as:
J Comp Neurol. 2010 April 15; 518(8): 1370–1390. doi:10.1002/cne.22282.

Regional Heterogeneity in Astrocyte Responses Following Contusive Spinal Cord Injury in Mice

Robin E. White[2,3], **Dana M. McTigue**[2,3,4], and **Lyn B. Jakeman**[*,1,2,3,4]

[1]The Ohio State University Department of Physiology and Cell Biology, Columbus, OH, 43210, USA

[2]Neuroscience Graduate Studies Program, The Ohio State University, Columbus, OH, 43210, USA

[3]The Center for Brain and Spinal Cord Repair, The Ohio State University, Columbus, OH, 43210, USA

[4]The Ohio State University Department of Neuroscience, Columbus, OH, 43210, USA

Abstract

Astrocytes and their precursors respond to spinal cord injury (SCI) by proliferating, migrating, and altering phenotype. This contributes to glial scar formation at the lesion border and gliosis in spared gray and white matter. The present study was undertaken to evaluate astrocyte changes over time and determine when and where interventions might be targeted to alter the astrocyte response. Bromodeoxyuridine (BrdU) was administered to mice three days after SCI, and cells expressing BrdU and the astrocyte marker, glial fibrillary acidic protein (GFAP), were counted at 3, 7, and 49 days post injury (DPI). BrdU-labeled cells accumulated at the lesion border by 7 DPI and approximately half of these expressed GFAP. In spared white matter, the total number of BrdU+ cells decreased, while the percentage of BrdU+ cells expressing GFAP increased at 49 DPI. Phenotypic changes were examined using the progenitor marker, nestin, the radial glial marker, brain lipid binding protein (BLBP), and GFAP. Nestin was upregulated by 3 DPI and declined between 7 and 49 DPI in all regions, and GFAP increased and remained above naïve levels at all time points. BLBP increased early and remained high along the lesion border and spared white matter, but was expressed transiently by cells lining the central canal and in a unique population of small cells found within the lesion and in gray matter rostral and caudal to the border. The results demonstrate that the astrocyte response to SCI is regionally heterogeneous, and suggests astrocyte populations which could be targeted by interventions.

Keywords

progenitor cell; central canal; nestin; brain lipid binding protein

Introduction

Contusive spinal cord injury (SCI) results in a cascade of cellular events, including the proliferation, migration, and hypertrophy of astrocytes (Frisen et al., 1995a; Rothstein et al., 1996; Lee et al., 1998; Krenz and Weaver, 2000; Ikeda et al., 2001; Costa et al., 2002; Tom et al., 2004; do Carmo Cunha et al., 2007). Astrocytes contribute to the formation of a glial scar at the lesion border, which functions as a physical and chemical barrier to axonal

[*]Corresponding Author Dr. Lyn B. Jakeman 401 Hamilton Hall 1645 Neil Avenue Phone: 614-688-4424 Fax: 614-292-4888.

regeneration (reviewed in Reier et al., 1983; Liuzzi and Lasek, 1987; Rudge and Silver, 1990; reviewed in White and Jakeman, 2008). In addition, astrocytes in spared gray and white matter undergo hypertrophy or gliosis after injury, a response that continues throughout the prolonged period of Wallerian degeneration (Buss et al., 2003; reviewed in Liberto et al., 2004). While these events are considered detrimental to axonal regeneration, recent studies have established that astrocyte proliferation and migration also serve an essential neuroprotective role (Faulkner et al., 2004; Okada et al., 2006; Hermann et al., 2008; Rolls et al., 2008). One goal of current research is to identify and target specific aspects of the complex astrocyte response in order to reduce the effects which inhibit regeneration while enhancing the beneficial functions of these cells (reviewed in Renault-Mihara et al., 2008; reviewed in White and Jakeman, 2008). Understanding the time course and regional differences in astrocyte proliferation and phenotype after injury is important in order to devise these approaches.

Astrocytes responding to SCI arise from a variety of sources, including mature cells near the lesion and progenitors that reside both in the parenchyma and in the ependymal zone surrounding the central canal (Johansson et al., 1999; Yamamoto et al., 2001; Mothe and Tator, 2005; Wu et al., 2005; Horky et al., 2006; Meletis et al., 2008; Sellers et al., 2009). The peak of cell proliferation occurs in the first week after a contusive SCI, and newborn neural progenitor cells differentiate almost exclusively into glial cells (McTigue et al., 2001; Lytle and Wrathall, 2007; Mothe et al., 2008). Although several recent studies have described the distribution of cells born early after SCI, most have focused on the chronic fate of these cells and the events associated with differentiation of those that proceed along the oligodendrocyte lineage (McTigue et al., 2001; Zai and Wrathall, 2005; Lytle et al., 2006; Yang et al., 2006; Tripathi and McTigue, 2007; Lytle et al., 2009). In contrast, there is less known about the time course and regional distribution of cells that go on to comprise the glial fibrillary acidic protein- (GFAP) expressing astrocytes, in part because of the lack of cellular markers that are specific for astrocyte precursor cells. In this study, we first used bromodeoxyuridine (BrdU) incorporation and unbiased cell counting to quantify the regional distribution of astrocytes born at 3 days after contusive SCI across a 3.0 centimeter block of tissue surrounding the lesion site. In contrast with a number of previous studies, the total numbers of labeled cells was determined using volumetric analysis spanning the full tissue block, thus facilitating comparisons over time that could be confounded by tissue shrinkage if they were reported as simple sample box density counts. These data show that early proliferating cells originate throughout the spinal cord. New astrocytes accumulate at the lesion border by 7 days after injury and do not increase further at later time points. In spared white matter, however, the number of BrdU+ cells decreases while the percentage of BrdU+/GFAP+ cells increases between 7 and 49 days after injury, indicating that the white matter glial response continues to evolve over time.

Astrocytes are heterogeneous cells and transcriptional control of their phenotype is dictated by local environmental cues (Kerr and Patterson, 2004; Ishii et al., 2006; Santos-Silva et al., 2007; reviewed in White et al., 2008). To define the time course and regional differences in the changes in astrocytes after SCI, the distribution of staining in the lesion border, spared gray matter, and spared white matter was compared by colocalization of cellular markers representing three important developmental stages of astrocytes: Nestin antibodies were used to identify progenitors and motile cells (Tohyama et al., 1992; Barry and McDermott, 2005), brain lipid binding protein (BLBP), an astrocyte-specific radial glial cell marker, was used to identify cells as soon as they are committed to an astrocyte lineage (Barry and McDermott, 2005; Schmid et al., 2006), and GFAP was used to identify mature, fully differentiated astrocytes. Photomicrographs and measurements of staining distribution patterns reveal that these three markers are regulated with different time course characteristics in the lesion border, spared gray matter and spared white matter regions. In

addition, this selection of markers revealed a previously undescribed population of round and unipolar BLBP+/ GFAP^{neg} cells that appears early after injury both in grey matter and in the ependymal zone surrounding the central canal. These cells may represent newly committed astrocytes that are born after SCI that can be selectively expanded or targeted for interventions.

Materials and Methods

Subjects

Adult female C57BL/6 mice 10 weeks of age weighing 17 to 20 g (Jackson Laboratories, Bar Harbor, ME) were housed in barrier cages in a temperature and humidity controlled room with *ad libidum* access to food and water. All animal experimentation procedures were performed according to approved protocols and in accordance with the NIH *Guide to the Care and Use of Laboratory Animals*.

Spinal Cord Injury

Mice were anesthetized with an intraperitoneal (i.p.) injection of ketamine (80 mg/kg; Vedco, St. Joseph, MO) and xylazine (10 mg/kg; Ben Venue Laboratories, Bedford, OH) and a thoracic level 9 (T9) laminectomy was performed under aseptic conditions. The Ohio State University Electromagnetic Spinal Cord Injury Device (OSU ESCID) was used to administer a moderate (0.5 mm displacement) contusion injury as described previously (Jakeman et al., 2000; Ma et al., 2001). After impact, the overlying muscles were sutured with 4–0 sutures. Skin openings were closed with vicryl sutures and the mice were allowed to recover in warmed cages overnight. Age-matched naïve mice were used as histological controls.

Post Operative Care

Bladders were expressed twice daily for the duration of the experiments. Throughout the study, mice were given peanut butter and sweetened cereal once daily to minimize weight loss after injury. To prevent urinary infections, subcutaneous injections of the antibiotic Gentamicin (5 mg/kg; Vedco) and 0.9% saline (1–3 cc) were administered for each day for 5 days after injury. Mice were given acidified (pH 5.5–6.0) water for the duration of the study.

Groups and BrdU Administration Paradigms

Progression of Early Proliferating Cells—This experiment examined the fate of cells proliferating on day 3 after contusion injury, corresponding to the peak of proliferation following SCI (Zai and Wrathall, 2005). All mice received a single bromodeoxyuridine pulse (BrdU; 50 mg/kg; Roche, Basel, Switzerland) given i.p. at 3 days post injury (DPI). Mice were perfused either 2 hours after BrdU injection (3 DPI), 4 days after BrdU injection (7 DPI) or 7 weeks after BrdU injection (49 DPI) (n=5 injured and 2 naïve mice per time point) (Figure 1A).

Acute Marker Expression—Mice in this experiment were used to examine astrocytic marker expression at very early time points following injury. The mice received moderate contusion injuries (as described above) and were perfused either 6 (n=3) or 24 (n=4) hours post injury (HPI) (Figure 1A').

Tissue Preparation

Mice were anesthetized at the indicated survival time with a lethal i.p. dose of ketamine (120 mg/kg) and xylazine (15 mg/kg), and then transcardially perfused with a 0.1 M phosphate buffered saline (PBS; pH 7.4) solution and then with 4% paraformaldehyde in 0.1 M PBS.

Spinal cords were post-fixed in 4% paraformaldehyde for 2 hours at 4°C and then placed in 0.2 M phosphate buffer (PB) for 24 hours at 4°C. Tissues were then submerged in 30% sucrose for 2–5 days for cryoprotection. Spinal cords were cut and frozen as 0.8 cm blocks centered on the laminectomy site in groups containing specimens from all of the time points. Serial transverse cryostat sections of 10 μm thicknesses were cut through the entire length of the block and saved in 10 sets of sections spaced 100 μm apart.

One set of sections was stained with eriochrome cyanine (EC, Sigma Aldrich, St. Louis, MO) to determine the distribution of residual myelin and to identify the epicenter of the injury, defined as the section with the least amount of white matter sparing (WMS) (Basso et al., 1996; Ma et al., 2001). The remaining sections were stored at −20°C and used for subsequent immunohistochemistry.

Immunohistochemistry for Brightfield Microscopy

All antibodies are described in Table 1. For the cell counting experiment, sections were stained with diaminobenzidine (DAB) and examined by brightfield microscopy. For BrdU immunohistochemistry, sections were pretreated in 2N HCl in dH_2O for 25 minutes at 37°C. After quenching endogenous peroxidases with H_2O_2 in methanol, tissues were incubated in blocking solution (0.1% Triton X-100/4% bovine serum albumin in 0.1 M PBS) for 20 minutes, then for 2 hours at room temperature with rat anti-BrdU diluted in the blocking solution (1:100, AbD Serotec, Raleigh, NC). The slides were then incubated with biotinylated rabbit anti-rat IgG (1:200, Vector Laboratories, Burlingame, CA) and then in Avidin-Biotin Peroxidase Complex (ABC Elite, Vector Labs, Burlingame, CA). 3,3'diaminobenzidine (DAB, Vector) substrate was added in the presence of H_2O_2, yielding a brown reaction product, and one set of slides was immediately dehydrated and cover slipped with Permount mounting medium (Fisher Scientific, Pittsburgh, PA). An additional set of sections was sequentially stained with rat anti-BrdU and rabbit anti-GFAP to identify astrocytes that arose at the time of BrdU exposure. After BrdU-DAB, the sections were incubated with blocking solution for 1 hour and then with rabbit anti-GFAP (1:1000, overnight at 4'C; Dako, Carpinteria, CA), biotinylated goat anti-rabbit IgG (1:1000, Vector), ABC Elite, and H_2O_2 with SG substrate (Vector Labs) to produce a grey reaction product (McTigue et al., 2001;Tripathi and McTigue, 2007).

Immunofluorescence

To examine the distribution and phenotype of astrocytes and their precursors, equally spaced sections were incubated either together or sequentially with primary antibodies raised against BrdU, nestin and BLBP (together), or nestin, brain lipid binding protein (BLBP) and GFAP (sequentially), and detected using three color immunofluorescence. Sections labeled with BrdU were first treated with 2N HCl and blocking solutions as described above. For chicken antibodies, 1% Blokhen II was added to the blocking solution. Sections were then overlaid with primary antibodies (rat anti-BrdU, proliferating cells, 1:800, AbD Serotec; rabbit anti-GFAP, astrocytes, 1:2000, Dako; chicken anti-GFAP, astrocytes, 1:100, Aves Labs, Tigard, OR; rabbit anti-BLBP, reactive astrocytes and radial glial cells, 1:2000, Millipore, Billerica, MA; chicken anti-nestin, progenitor cells, 1:100, Aves Labs), diluted in the appropriate blocking solutions. The sections were then incubated with Alexafluor secondary fluorescent antibodies (Invitrogen, Carlsbad, CA; goat anti-rabbit 488; goat anti-rabbit 546; goat anti-chicken 647; goat anti-rat 546). Sections were then rinsed with 0.1 M PBS and cover slipped with Immumount (Thermo Scientific, Pittsburgh, PA).

For sections labeled with both rabbit anti-GFAP and rabbit anti-BLBP, the sections were incubated first with the optimal dilution of rabbit anti-BLBP and the appropriate secondary antibody, followed by an additional blocking and rinsing steps, and were then incubated

with rabbit anti-GFAP followed by its secondary antibody. Negative controls absent of either primary antibody were performed to determine the specificity of staining using these antibodies and staining protocol. The controls revealed that, both in white matter regions with little BLBP immunoreactivity and at the lesion epicenter where BLBP immunoreactivity was extremely high, no cross-reactivity was present (Supplemental Figure 1). To further confirm the patterns of colocalization, selected sections were incubated with rabbit anti-BLBP and chicken anti-GFAP (Aves Laboratories). Similarly, for triple-labeling with rat, rabbit, and chicken primary antibodies, controls were performed where each of the primary antibodies was omitted and all secondary antibodies applied, and negative controls exhibited no signal (data not shown).

Antibody Characterization

Information on the source and dilutions for all antibodies is described in Table 1.

The rabbit polyclonal anti-brain lipid binding protein (BLBP) antibody (Millipore, catalog #AB9558, lot #LV1449719) was raised against recombinant whole mouse BLBP. It reacts with a single band at approximately 15 kDa on western blot as expected and is specific to embryonic radial glia and postnatal astrocytes (manufacturer's technical information). Patterns of staining matched that of previously published patterns (Barry & McDermott, 2005).

The rat monoclonal anti-bromodeoxyuridine (BrdU) antibody (AbD Serotec, catalog #MCA2060) was produced by clone BU1/75 (ICR1), and raised against BrdU. The antibody reacts with single-stranded BrdU, BrdU attached to a carrier protein, and free BrdU, but not thymidine (manufacturer's technical information). We verified that the antibody does not yield staining in spinal cord injured mouse tissue not injected with BrdU.

The polyclonal rabbit anti-glial fibrillary acidic protein (GFAP) antibody (Dako, catalog #Z0334, lot #096) is a purified IgG fraction of rabbit antiserum raised against GFAP isolated from cow spinal cord. The antibody identifies one distinct precipitate using crossed electrophoresis, labels astrocytes in the mature nervous system, and reacts with mouse GFAP (manufacturer's technical information), but does not react with human or cow serum proteins. Staining observed in injured tissue was similar to that previously reported (Vijayan et al., 1990).

The polyclonal chicken anti-nestin antibody (Aves Laboratories, catalog #NES, lot # NES0305) was raised against three different synthetic peptide conjugates (described in Table 1). The antibody reacts with a band of approximately 265 kDa using western blot on mouse brain and identifies radial glial cells in mouse embryonic day 13.5 brain (manufacturer's technical information). The antibody identifies patterns similar to those previously reported after spinal cord injury (Clarke et al., 1994). In addition, the antibody colocalizes with a monoclonal mouse anti-nestin antibody (mouse anti-Rat 401 nestin, Developmental Studies Hybridoma Bank).

BrdU+ and BrdU+/GFAP+ Sampling Paradigm and Cell Counting

To determine the distribution of BrdU+ and BrdU+/GFAP+ profiles in selected regions of the injured spinal cord, profiles in sample areas (0.16 mm^2 area) of sections labeled with BrdU and GFAP in DAB and SG, respectively, were manually counted using a Zeiss Axioplan microscope with a 40× objective and 10× eyepiece with a sample box outline.

Images were obtained from equally spaced sections at 200 μm intervals from 1.4 mm rostral to 1.4 mm caudal from the lesion epicenter, resulting 15 sections per animal (Figure 1B), spanning a counting volume of 3.0 mm. Tagged image file format (TIFF) images of the EC-

stained and anti-BrdU/GFAP sections were collected with the MCID™ Image Acquisition Software (previously Imaging Research, now InterFocus Imaging Ltd, Cambridge, UK) as previously described, and imported into a presentation software (Microsoft Powerpoint) for preparation of working maps.

The EC-stained images were used to outline the lesion edge, which was defined in every section as the best line separating relatively intact grey and white matter from damaged tissue areas that were devoid of any myelin stain (dashed line and *, Figure 1C, top). The spared white matter regions (SWM, +) were defined as areas which exhibited dense blue staining and contained profiles resembling myelin rings; spared grey matter (SGM, #) was defined as areas in which light EC staining and outlines of spared neurons could be discerned, and the lesion border region was defined as the area immediately adjacent to and inside the lesion edge apposing either SWM or SGM (Figure 1D). These EC-defined border maps were then superimposed upon images of adjacent sections labeled with anti-BrdU and GFAP to establish sampling maps for manual counting (Figure 1C, bottom). Counting boxes were evenly distributed on the maps so that the SWM samples (red boxes) and SGM samples (blue boxes) were distributed throughout the regions of interest, but did not encroach within 1 box width (0.4 mm) of the lesion edge, as described previously (Tripathi and McTigue, 2007). Lesion border samples (green boxes) were then placed along the inside lesion edges.

In each of the defined sample regions, BrdU+ and BrdU+/GFAP+ profiles were manually counted in microscopy sample fields of 0.16 mm^2 from sections double-labeled with BrdU and GFAP as viewed on the Zeiss Axioplan with a 40× objective and 10× eyepiece. The field of view was aligned to match each of the sampling boxes on the lesion maps. BrdU+ profiles were counted in the sample field if a clear brown reaction product with nuclear morphology was present (arrows and arrowheads, Figure 1E). Double labeled BrdU+/GFAP + profiles were counted only if at least three quarters of the BrdU+ nucleus was surrounded by a GFAP+ cytoskeleton (arrows, Figure 1E; Tripathi and McTigue, 2007). Confirmation of double-labeling required focusing through the full height of the tissue section.

Determination of tissue region area and reference volume

To determine the reference area per section and reference volume of the lesion border, spared white matter, and spared grey matter over time, the Cavalieri method was used (Rosen and Harry, 1990; Beck et al., 1993). A transparency with a grid containing points spaced 8.2 mm apart was randomly placed on top of the image maps, and the number of grid points aligned with SWM, SGM, and lesion border regions were counted. Grid counts were then multiplied by a/p (a/p = area of the point on the transparency grid, a/p = 0.029184 mm^2), which yielded an approximate area for each region and section ($A_{section}$). These values were then multiplied by 20 to account for thickness between sections and summed to estimate the total reference volume of each region: $V = \Sigma (A_{section} \times 200\ \mu m/10\ \mu m)$. From 3 to 49 DPI, there was no significant change in spared grey matter or lesion border volume, but there was a significant decrease in the volume of spared white matter at 49 DPI (Figure 1F).

Corrections and summation of profile counts

Because profile cell counts inherently result in over-counting (reviewed in Guillery, 2002), an Abercromie correction factor was applied to the BrdU+ profile counts. This correction factor was calculated by dividing the thickness of the section (10 μm) by the thickness of the section added to the average height of the profiles ($t / t+h$, where t = tissue thickness and h = average cell height). The average BrdU+ profile height was determined separately in each tissue region by measuring the diameter of 30 cells in sections from tissue from a related

study that was cut longitudinally (perpendicular to the transverse sections in this study) and processed identically to the above described sections. The correction yielded BrdU+ profile heights of 7.1 μm, 8.7 μm, and 7.9 μm and associated correction factors of 0.5850, 0.5345, and 0.5597 for lesion border, spared white matter, and spared grey matter, respectively. All averaged profile counts were therefore multiplied by the appropriate correction factor to determine the numbers of BrdU+ cells.

The number of BrdU+ and BrdU+/GFAP+ profiles per region was then determined by averaging the corrected profile counts of the sample areas in each section and multiplying these sample counts by the reference area for the section (above) divided by the sample box area of each section: $C_{\text{section}} = C_{\text{sample box}} \times A_{\text{section}}/A_{\text{sample box}}$. Next, this section value was multiplied by 20 to estimate the total number of cells present between each tissue section (10 μm thick sections placed 200 μm apart). These values were then added together to derive the total number of cells over the volume spanning the entire 3.0 mm length of spinal cord. To compare changes rostral and caudal to the lesion epicenter, the cell counts were further divided into three tissue blocks (Figure 1B). The “rostral” region (R) included sections spanning 1.4 mm rostral to the epicenter to <0.4 mm rostral to the epicenter, the “epicenter” region (E) spanned 0.4 mm rostral to the epicenter to <0.4 mm caudal to the epicenter, and the “caudal” region (C) spanned 0.4 mm caudal to the epicenter to <1.4 mm caudal to the epicenter.

Quantification of Marker Expression

To quantify changes in patterns of BLBP, GFAP, and nestin expression in the lesion border, spared grey matter, and spared white matter, a Zeiss 510 Laser Confocal Microscope (The Ohio State University Confocal Microscopy Imaging Facility (CMIF)) was used to gather single and merged images of each region at the injury epicenter, 1.0 mm rostral from the epicenter, and 1.0 mm caudal from the epicenter. The confocal detection and pinhole settings were established by setting thresholds to accurately reflect known staining patterns present in tissue sections from naïve controls. Images of BLBP, GFAP, and nestin immunoreactivity were then collected from three sites per region at 63× magnification, at the epicenter and 1.0 mm rostral and caudal from the epicenter for each subject. The images were then imported into the MCID analysis program to measure the sample area (SA) of immunoreactivity for each marker as a function of total staining in the corresponding “merged” image: $\textit{Proportional Area}_{\text{stain}} = SA_{\text{stain}} / SA_{\text{merged}}$.

Quantification of BLBP+ cells expressing GFAP

BLBP is a cytoplasmic protein present in astrocytic cells. The regional analyses revealed a population of distinct BLBP+ cells that appeared at 6 HPI to 3 DPI in the lesion core and rostral and caudal gray matter. To determine the proportion of these BLBP+ cells expressing GFAP over time in various regions, clearly defined BLBP+ profiles were manually identified using the Zeiss Axioplan microscope with a 40× objective and 10× eyepiece with a fluorescent filter capable of viewing emission wavelengths of 488 nm (green) and 546 nm (red). The images created for volume analysis were used as a reference to define the lesion core (absent of any spared tissue), lesion border, spared white matter, and spared grey matter, similar to the BrdU+/GFAP+ profiles counts.

BLBP+ profiles were identified in each of these regions at the injury epicenter, 1.0 mm rostral from the lesion epicenter, and 1.0 mm caudal from the lesion epicenter. A total of 6–12 BLBP+ profiles were counted in the lesion core, lesion border, and spared white and grey matter across 3 sections at each distance from the epicenter. Areas with fewer than 6 BLBP+ cells were omitted from data analysis. BLBP+ profiles were counted if they exhibited a distinct, solid red profile (cytoplasmic staining of BLBP). BLBP+/GFAP+ cells were

defined as any BLBP+ cell exhibiting GFAP immunoreactivity overlapping the BLBP signal or clearly surrounding the BLBP+ nucleus. These counts were used to estimate a percentage of BLBP+ cells not expressing GFAP in each region for each subject at all time points.

Quantification of Proliferating BLBP+/GFAP^{neg} Cells

To estimate the proportion of BrdU+ cells that were BLBP+/GFAP^{neg} cells at 3 DPI, a total of 18 BrdU+ profiles were identified in the lesion core from three sections spanning the lesion epicenter block. The number of these cells expressing BLBP was manually determined and the proportion of BrdU+ cells expressing BLBP was calculated by dividing the number of BrdU+/BLBP+ cells by the total number of BrdU+ cells. To estimate the percentage of BrdU+ cells surrounding the central canal expressing BLBP, the total number of BrdU+ cells adjacent the central canal was counted from 0.7–0.9 mm rostral and caudal from the lesion epicenter and the number of these cells expressing BLBP was determined. The proportion of BrdU+ cells expressing BLBP was determined by dividing the number of BrdU+/BLBP+ cells by the total number of BrdU+ cells.

Brightfield and Fluorescent Photomicrographs

Images for documentation were chosen by closely examining areas in all subjects at all time points, and representative images were taken using the Zeiss Axioplan and MCID or Zeiss 510 Confocal Microscope. For preparation of manuscript figures, Adobe Photoshop (CS2) was used to adjust brightness, contrast, and sharpness of images with identical settings for all panels. Alterations were not performed on images used for quantitative purposes. Figures were assembled using Adobe Photoshop.

Statistical Analysis

GraphPad Prism 4.0 was used for statistical analysis. Two-way ANOVAs comparing region and time point were used to analyze tissue volume, BrdU+, BrdU+/GFAP+, percentage of BrdU+ cells that were astrocytes, percentage of BLBP+ cells expression GFAP, marker expression over time, and Bonferroni post hoc tests were used to determine specific differences between time points and regions in ANOVAs. Significance was set at $p < 0.05$. For all figures, error bars represent standard error of the mean (SEM).

Results

Regional differences in the distribution of newborn astrocytes over time

Past studies have shown that early proliferating cells accumulate at the lesion border over time following spinal cord contusion injury (Tripathi and McTigue, 2007). The time course and sampling paradigm of the following experiments are shown in Figure 1. To discern the time course of this accumulation and the proportion of these cells that become astrocytes, BrdU+ and BrdU+/GFAP+ profiles were counted within the defined lesion border region at 7 and 49 DPI (Figure 2). At 3 DPI, the lesion site is characterized by an accumulation of GFAP+ debris, but very few distinct GFAP+ cells are observed, and a defined lesion border is not present (Figure 2A). Single and double labeled cells were abundant in this region at both 7 and 49 DPI (Figure 2B,C). The lesion border is primarily restricted to the epicenter block spanning 0.4 mm rostral to <0.4 mm caudal to the epicenter. By 7 DPI, there is an accumulation of BrdU+ cells in this region, almost half of which are GFAP+ astrocytes (Figure 2D–F). Both the number of BrdU+ and the number of BrdU+/GFAP+ cells remains constant at 49 DPI, suggesting that early proliferating cells make their contribution to the astrocyte population in this region in the first week following injury and do not continue to proliferate.

Recent studies have indicated that astrocytes and precursors in spinal gray matter are capable of proliferation after injury (Yamamoto et al., 2001; Zai and Wrathall, 2005; Lytle and Wrathall, 2007; Buffo et al., 2008), but the numbers of these cells and the time course of their differentiation are not known. As expected, naïve tissue exhibited little to no proliferation (data not shown). With administration of BrdU at 3 DPI, BrdU+ and BrdU+/GFAP+ cells were found in the spared gray matter as early as 2 hours after BrdU injection, indicating that GFAP+ expressing cells in this region indeed participate in early proliferation (Figure 3A–C). Greater total cell numbers in the rostral and caudal blocks primarily reflect the absence of spared gray matter in the epicenter region (Figure 3D–E). From 3 to 49 DPI, there was no change in the total number of BrdU+ cells in grey matter, indicating that continued proliferation of cells is minimal. The total numbers of BrdU+/GFAP+ cells revealed a slight increasing trend toward astrocyte differentiation over time; this finding was not significant. However, expression of the percent of the BrdU+ cells in the gray matter that express GFAP significantly increased from approximately 20%–40% over time (two-way ANOVA, $p < 0.001$; Figure 3F).

Like grey matter, naïve white matter exhibited little to no proliferation (data not shown). After injury, BrdU+ and BrdU+/GFAP+ cells were also found in spared white matter regions as early as 3 DPI and readily identified at 7 and 49 DPI (Figure 4A–C). Again, more BrdU+ cells were found within the rostral and caudal tissue blocks where white matter sparing was greater, as described above (Figure 4D). Unlike the lesion border or spared grey matter, however, the number of BrdU+ cells in spared white matter decreased from 3 to 49 DPI in both the rostral and caudal tissue blocks (Figure 4D), indicating a loss of cells born at 3 DPI. On the other hand, over the same time period, the number of BrdU+/GFAP+ cells in the spared white matter regions increased (Figure 4E). In turn, the percentage of BrdU+ cells expressing GFAP increased from 20–25% of all BrdU+ cells at 3 DPI to as many as 70–80% of the remaining BrdU+ cells at 49 DPI.

Regional differences in astrocyte marker expression over time

GFAP is an intermediate filament protein that is a time-honored astrocyte marker (Eng et al., 1971; Bullon et al., 1984). However, GFAP expression is initiated fairly late in astrocyte maturation (Eng et al., 1971; Barry and McDermott, 2005), and detailed understanding of sources of astrocytes and their time course of differentiation after injury have been hampered by the lack of specific early markers of these cells. In order to obtain a picture of astrocyte activation and maturation after injury, we employed three markers that are expressed by cells of the astrocyte lineage: Nestin is expressed by a wide range of undifferentiated cells and by mature astrocytes, and was used to identify progenitors and other highly motile cells (Toyhama et al., 1992; Kleeberger et al., 2007). BLBP is upregulated in response to notch signaling, and is expressed specifically in radial glial cells that are committed to an astrocytic fate (Anthony et al., 2005; Barry and McDermott, 2005; Schmid et al., 2006). Finally, GFAP was used to identify mature and reactive astrocytes and to compare staining patterns with a large body of existing literature.

In uninjured spinal cord, astrocytes in both grey and white matter express low levels of GFAP. In contrast, BLBP expression is restricted to a small number of cell bodies in grey matter, a few cell bodies in the superficial dorsal horn, and cells contacting the pia in the periphery of the white matter. Nestin is expressed at very low levels in grey matter and in cells contacting the pia in white matter.

In the area that will develop into the lesion border region, GFAP expression at 3 DPI is associated with cellular debris and few astrocytes can be discerned (Figure 5A, see also Figure 2A). By 7 DPI, however, the lesion border is discerned and GFAP expression is prominent throughout the border (Figure 5B, 5E, 2B). Nestin expression is markedly

upregulated at both 3 and 7 DPI, but its distribution changes between these time points. Nestin is only partially colocalized with GFAP at 3 DPI, and more completely colocalized at 7 DPI. BLBP expression remains low at 3 DPI and increases strongly by 7 DPI, when it is nearly perfectly colocalized with GFAP and nestin (Figure 5A', A"). By 49 DPI, when the glial scar is fully formed, both GFAP and BLBP expression remain high, but nestin expression decreases dramatically (Figure 5C). A quantitative comparison of the marker expression patterns over time was conducted by determining the total area of staining in triple stained, merged images (i.e. Figure 5A'", B'" and C'"), and measuring the average proportion of this area contributed by each of the three markers (Figure 5D). This analysis shows that GFAP expression corresponds to 60–80% of total marker staining in the lesion border regions from 3 – 49 DPI. In contrast, BLBP expression does not increase substantially until 7 DPI, corresponding to the establishment of the glial border. Nestin expression is high by 3 DPI, but returns to naïve levels by 49 DPI.

Spared grey matter regions rostral and caudal to the lesion epicenter also revealed differences in marker expression over time (Figure 6). At 3 DPI, GFAP revealed hypertrophied astrocytes, and this staining pattern was relatively unchanged over time. BLBP expression remained similar to that of naïve tissue at 3 DPI, but nestin expression is increased at this time. Most nestin+ profiles colocalize with GFAP, but some nestin+/GFAP^{neg} profiles can also be found (Figure 6B). By 7 DPI, BLBP expression is significantly increased, while nestin expression decreases to naïve levels (Figure 6C). At 49 DPI, BLBP levels return to normal and nestin levels are slightly below that of naïve tissue (Figure 6D). Quantitation of the staining patterns illustrate the different time course of expression of the three markers, emphasizing peak expression of nestin at 3 DPI and BLBP at 7 DPI, but both of these markers comprise very little of the total staining area by 49 DPI.

In spared white matter of naïve spinal cord, GFAP is found at low levels throughout the white matter, while BLBP is expressed only in cells directly apposed to the peripheral pial border (Figure 7A–A'"). At 3 DPI, there is little change in astrocyte morphology, but nestin expression is significantly higher than in uninjured specimens (Figure 7B). Unlike the lesion border and gray matter, all of the nestin+ profiles were colocalized with GFAP. At 7 DPI, astrocytes throughout the white matter showed a hypertrophied morphology and increased BLBP expression, while nestin levels were unchanged from 3 DPI (Figure 7C). By 49 DPI, BLBP expression remained elevated and closely correlated with GFAP, while nestin expression had decreased to naïve levels (Figure 7D).

BLBP+/GFAP^{neg} cells are present in the lesion core and border early after SCI

At 3 DPI, in both the debris of the lesion core and in spared grey matter rostral to the injury epicenter, we observed small BLBP+/GFAP^{neg} cells exhibiting a unique morphology unlike that of mature, GFAP-expressing astrocytes (Figure 8A). At this time point, these cells usually had a rounded cell body with either no processes or a single process, and some of these cells also expressed nestin (Figure 8B [nestin+],C [nestin^{neg}]). Careful examination of the cells did not reveal any identifiable patterns to explain this discrepancy in nestin expression. A subset of these cells was labeled with BrdU, indicating that they represented newborn cells that appear to be rapidly committed to an astrocyte lineage (figure 8D,E). To determine the contribution these cells were making to the total number of BrdU+ cells present at 3 DPI, the percentage of BrdU+ cells in the lesion core at the injury epicenter was calculated, revealing that approximately 77% of BrdU+ cells in the epicenter were BLBP+ (Figure 8D–E). These cells were never detected in spared white matter. By 7 DPI, these cells were not present in any region examined (Figure 8F–I).

Although the peak of proliferation occurs at 3 DPI, dividing progenitors in spinal cord parenchyma have been shown to be present earlier after injury (Yamamoto et al., 2001;

Sellers et al., 2009). To determine if the unique BLBP+/GFAP^{neg} cells were present prior to 3 DPI, additional animals were injured and perfused 6 and 24 hours post injury (HPI). BLBP +/GFAP^{neg} cells were present in both the lesion core and spared grey matter as early as 6 and 24 HPI (Supplemental Figure 2A,B). At these early time points, all BLBP+/GFAP^{neg} cells exhibited a rounded morphology devoid of processes. At 6 HPI, none of these cells expressed nestin, while some did at 24 HPI.

BLBP+/GFAP^{neg} cells surround the central canal early after injury

Several studies have shown that, especially after minimal SCI, the cells surrounding the central canal undergo proliferation (Mothe and Tator, 2005; Meletis et al 2008) and have potential to become mature astrocytes (Meletis et al., 2008). Based on these data, we hypothesized that this area might also exhibit unique expression of the early astrocyte/radial glial marker BLBP. Naïve spinal cord contains a subset of GFAP+ astrocytes near the central canal, but none of the cells directly lining the canal express GFAP, BLBP or nestin (Figure 9A–A'''). At 3 DPI, however, BLBP and nestin are both strongly upregulated in this population of cells (Figure 9B–B'''). Indeed, BLBP+/GFAP^{neg} and nestin+/GFAP^{neg} cells are present in this area as soon as 6 and 24 HPI (Supplemental figure 2C,D). The expression of BLBP and nestin in these cells peaks at 3 DPI, especially in regions approximately 0.7–0.9 mm rostral and caudal to the injury epicenter. By 7 and 49 DPI, BLBP expression immediately surrounding the central canal is reduced to that of naïve tissue (Figure 9C,D), while the surrounding cells adjacent to the lesion border maintain expression of BLBP and decrease expression of nestin chronically (Figure 9D). Similar to observations of BLBP+/GFAP^{neg} cells in the lesion core, some of these cells were also labeled with BrdU at 3 DPI, confirming that they were generated on the day of perfusion (Figure 9E–E"). Because robust proliferation occurs early after injury in this region in minimal SCI models, we calculated the percentage of BrdU+ cells lining the canal at 3 DPI that also expressed BLBP, revealing that approximately 88.9% and 71.4% of the dividing cells surrounding the central canal express BLBP 3 DPI rostral and caudal from the epicenter, respectively (Figure 9E). Thus, a small population of round and unipolar BLBP+ cells arise from the central canal region and surrounding grey matter early after injury. Some of these cells express nestin, while some do not, but by 7 DPI, all BLBP+ cells also express GFAP.

Discussion

Summary of main findings

Spinal cord injury (SCI) initiates a cascade of cellular events that induces the proliferation, migration, and alteration in phenotype of astrocytes. The complex astrocyte response contributes to neuroprotection while inhibiting axonal regeneration. However, it is not yet clear if the proliferation and differentiation of astrocytes can be targeted in a temporally and regionally restricted manner in order to modify the detrimental functions of these cells. This paper strove to address this question using two different approaches.

First, we used unbiased cell counting following a single pulse of bromodeoxyuridine (BrdU) administered to mice 3 DPI to identify the distribution of those cells that arise during the peak of endogenous cell proliferation. The BrdU was combined with glial fibrillary acidic protein (GFAP) immunohistochemistry, and the results represent the first documentation of the total number and the proportions of these cells that contribute to the early and chronic populations of GFAP+ astrocytes in the lesion border, spared grey matter and spared white matter regions at acute and chronic post-injury times. These results indicate that cells that are born during the wave of proliferation at 3 DPI do not undergo further substantial cell division, and by 1 week after injury, approximately half of them have differentiated into GFAP+ astrocytes. This percentage remains stable in the glial scar at the lesion border,

while the percentage of new cells expressing GFAP continues to increase in spared grey and white matter regions over time.

Second, we used a unique combination of the astrocyte-specific radial glial marker brain lipid binding protein (BLBP) together with nestin and GFAP immunofluorescence to compare the phenotypic profiles of cells of astrocyte lineage across different local environment regions. GFAP expression was increased by 3–7 DPI in all regions and remained high through 49 DPI, while nestin expression was upregulated everywhere early after injury, but decreased in all regions by 49 DPI, suggesting that a relative short time window exists for a widespread population of multipotent progenitors following SCI. In contrast, the time course of BLBP expression differed markedly across the three tissue regions, with early and sustained upregulation in the lesion border and spared white matter regions and transient expression in the central canal and spared gray matter. Notably, this staining combination also revealed a unique population of BLBP+/GFAP^{neg} cells surrounding the central canal and in the grey matter parenchyma early after injury, indicative of a new population of astrocyte precursor cells prior to their full differentiation into GFAP-expressing astrocytes.

Together, these findings demonstrate that astrocytes display regional specificity in response to signals associated with both the injury and the local microenvironment. The use of BLBP as a tool to distinguish astrocytes at their earliest stage of commitment to an astrocyte lineage will facilitate understanding the effects of therapies targeting the astrocyte response with the goal of improving repair after injury.

GFAP+ cells are generated after SCI

After neurogenesis and gliogenesis are completed during development, significant proliferation of neural progenitors in the mature central nervous system (CNS) is largely restricted to specific areas of the hippocampus (reviewed in Kempermann and Gage, 2000) and the subventricular zone of the brain (reviewed in Lennington et al., 2003). During the first week after SCI, there is robust wave of increased cell proliferation throughout the nearby spinal cord (Johansson et al., 1999; McTigue et al., 2001; Yamamoto et al., 2001; Zai and Wrathall, 2005; Horky et al., 2006; Lytle and Wrathall, 2007). To accurately estimate the total number of BrdU+ and BrdU+/GFAP+ cells in each region at each time examined, we calculated reference volume using transverse sections for each region and time point and found that white matter undergoes significant shrinkage over time, similar to previous data (Lytle and Wrathall, 2007). In addition, rostral-caudal shrinkage of the lesion between 1 and 4 weeks post injury has been documented after crush injury (Zhang et al., 1996), but no such analysis has been completed after contusion injury. Shrinking in multiple dimensions may result in an artifactual increase in the number of cells counted over time, but our data does not show an increase in total BrdU+ cells. Conversely, we documented a decrease in the number of BrdU+ cells over time in white matter, a region that exhibits significant shrinkage. Furthermore, measures of the proportion of BrdU+ cells expressing GFAP at each time point should not be affected by shrinkage and are an accurate portrayal of the composition of BrdU+ cells in each region.

When a single pulse of BrdU was administered at 3 days post injury (DPI) and the mice were perfused 2 hours later, similar total numbers of BrdU labeled nuclei were distributed through grey and white matter over several hundred microns rostral and caudal to the lesion epicenter. Many cells that incorporated BrdU at 3 DPI were concentrated at the rostral and caudal margins of the lesion, where surviving cells could be influenced by a wide range injury-related growth factors and cytokines (Widenfalk et al., 2001; Nakashima et al., 2005; Xu et al., 2006; Tripathi and McTigue, 2008).

Within the spared grey and white matter regions, 10–30% of the cells that incorporated BrdU expressed GFAP at 3 DPI. These results are consistent with similar studies and confirm that unlike mature oligodendroglia and neurons, a significant proportion of mature astrocytes in the spared tissue regions of the spinal cord can re-enter the cell cycle after injury (Yamamoto et al., 2001; Zai and Wrathall, 2005; Lytle and Wrathall, 2007; Buffo et al., 2008). The majority of early proliferating cells accumulate along the lesion border by 7 DPI and remain at the border at chronic time points, similarly shown in other injury models and species (Yang et al., 2006; Lytle and Wrathall, 2007; Tripathi and McTigue, 2007). Using the current analyses, we show that nearly half of these cells express GFAP+ by 7 DPI, a higher percentage than previously reported (Yang et al., 1996). These results suggest that the mouse spinal cord may have a greater bias toward astrocyte proliferation and/or chronic GFAP expression after injury than other species. A direct comparison of astrocyte genesis has not been performed, but previous work has shown that some characteristics of the inflammatory response and the final lesion composition in mice evolve differently from rats and other species (Kuhn and Wrathall, 1998; Jakeman et al., 2000; Sroga et al., 2003). Because the cellular responses are dictated largely by local intercellular interactions, it is reasonable to suggest that differences in the extracellular composition may enhance these astrocyte characteristics in mice. Dramatic differences in neuroprotection, inflammation and fibrosis are also evident between strains of mice (Inman et al., 2002;Kigerl et al., 2006), and we have described one common strain of mouse that has a unique phenotype including enhanced migration of astrocytes into the lesion epicenter after a contusion injury (Ma et al., 2004; White et al., 2008). Thus, complex genetic traits can contribute to a comparatively strong astrocyte proliferative response seen in the mouse.

An unexpected finding was that within the spared white matter regions, the total number of BrdU cells decreased rostral and caudal to the epicenter, but both the number and proportion of BrdU+/GFAP+ cells increased dramatically by 49 DPI. Three explanations are possible. First, the increased numbers of double labeled cells could reflect a late increase in GFAP expression by cells that were not fully activated at 3 and 7 DPI. A second factor contributing to the marked increase in the proportion of BrdU+ astrocytes in spared white matter is the chronic loss of other cell types. Oligodendrocytes undergo apoptotic cell death in long fiber tracts undergoing Wallerian degeneration for several weeks after contusive SCI (Abe et al., 1999). While new oligodendrocytes are generated within the spared white matter after contusion injury (Lytle and Wrathall, 2007; Tripathi and McTigue, 2007), the cell numbers here suggest that these non-GFAP+ populations do not survive well in the chronically injured white matter. Another explanation for the decrease in BrdU+ cells in spared white matter over time is delayed microglial death. Microglia divide early after injury (Yang et al., 2006) and undergo apoptosis chronically (Shuman et al., 1997), possibly contributing to the declining population observed in this study.

BLBP immunoreactivity reveals regional heterogeneity in astrocyte phenotypic response to SCI

The present study is the first to characterize the distribution of BLBP immunoreactivity over time in the injured rodent spinal cord. In the lesion border and spared white matter, BLBP expression was strongly upregulated and colocalized with GFAP expression, while in spared grey matter regions rostral and caudal to the lesion, BLBP expression was increased and then returned to naïve levels by 49 DPI. Although the specific stimuli for regulating BLBP expression after injury have not been determined, one candidate is the transcription factor, Reelin. Reelin is expressed in normal white matter (Hochstim et al., 2008) and may account for BLBP expression in this region in naïve tissue. Reelin is upregulated after ocular (Pulido et al., 2007) and nerve injury (Panteri et al., 2006), but its expression pattern has not been examined after SCI. The function of BLBP after injury is also unknown. BLBP is a member

of fatty acid binding protein family (FABP), a group that regulates metabolic processes (reviewed in Haunerland and Spener, 2004) and trafficking of intracellular ligands in the normal CNS (Feng et al., 1994). Other FABPs are upregulated after peripheral injury (De Leon et al., 1996), and knocking down FABP5 after SCI using siRNA results in impaired recovery (Figueroa et al., 2009).

BLBP expression revealed a unique population of BLBP+/GFAP^{neg} cells present primarily in the lesion core and surrounding the central canal from 6 hours post injury (HPI) to 3 DPI. Due to their uncharacteristic morphology (rounded or teardrop-shape) and a marker expression pattern resembling astrocyte-restricted radial glial cells, we have proposed that these cells might be precursors committed to differentiate into astrocytes. Cells expressing the transgene in a BLBP reporter mouse line include only radial glial cells in development and astrocytes in the mature CNS (Schmid et al., 2006). Definitive fate mapping of these cells after injury would require a similar transgenic mouse line with conditional expression of BLBP in the mature CNS to eliminate sustained expression from all astrocyte precursors in early development. However, a number of related observations provide indirect support for the implication that these cells represent astrocyte precursors. Within spared grey matter, neither the number of BrdU+ or BrdU+/GFAP+ cells increased from 3 to 7 DPI, indicating that the newborn BLBP+ cells did not die in significant numbers. By 7 DPI, however, BLBP +/GFAP^{neg} cells were no longer present, but BLBP expression continued to increase and all BLBP expression was fully colocalized with GFAP, similar to the pattern of axonal-supportive differentiation that is reported after spinal cord injury in the adult turtle (Rehermann et al., 2009). The time course of BLBP+ expression in GFAP^{neg} ependymal cells also corresponds closely with the known proliferation and migration of these cells that have been shown to differentiate into astrocytes after injury (Frisen et al., 1995b; Johansson et al., 1999; Namiki and Tator, 1999; Mothe and Tator, 2005; Meletis et al., 2008).

In the lesion core, GFAP expression at 3 DPI is primarily in the form of astrocytic debris. However, nestin is upregulated throughout the lesion at this time and is present in some BLBP+/GFAP^{neg} cells in the lesion core and the lesion border regions. Nestin is a progenitor marker that is not specific for astrocytes. Additional nestin+ cells not expressing GFAP or BLBP were also noted, and these are very likely to include well described glial progenitors that express the chondroitin sulfate proteoglycan, neuro-glial antigen 2 (NG2) (Burns et al., 2008). Some of these nestin+ cells would be expected to express the transcription factor Olig2 and will go on to form oligodendrocytes (Horky et al., 2006; Yang et al., 2006; Tripathi and McTigue, 2007; Burns et al., 2008; Lytle et al., 2009). Alternatively, some NG2+ cells born early after injury can develop into protoplasmic astrocytes, defined by their co-expression of S100β+ and the glutamate transporter, GLAST and the lack of expression of GFAP (Zhu et al., 2008a; Zhu et al., 2008b; Lytle et al., 2009; Sellers et al., 2009). We were unable to co-stain tissue sections with specific labeling using BLBP and NG2 antibodies in the lesion core at 3 DPI. However, the present study showing robust colocalization of BLBP and GFAP by 7 DPI suggest that the BLBP+/GFAP^{neg} cells described at 6 HPI to 3 DPI are distinct from previously described NG2+ progenitors and may well add a new population to the previously known sources of GFAP+ astrocyte precursor cells.

Conclusions and Significance

In past studies, substantial research has been conducted on the proliferation and differentiation of oligodendrocytes and their progenitors (Tripathi and McTigue, 2007; Lytle and Wrathall, 2007), in part because of their potential to remyelinate damaged axons after injury. The current study extends these findings with a focus on the proliferation and distribution of astrocytes and astrocyte precursors after injury. While astrocytes are typically targeted due to their role in the formation of the glial scar, they also perform a variety of

other functions vital for successful endogenous repair, such as rebuilding the blood-brain barrier (Whetstone et al., 2003) and reducing excitotoxicity (Rothstein et al., 1996). The development of therapeutic strategies aimed at manipulating astrocytes must begin with a solid foundation of knowledge on the endogenous astrocyte response to injury. In this study, we have provided evidence showing that astrocytes arise after injury from GFAP+ expressing cells in grey and white matter as well as precursors found within the lesion center, ependymal region, and surrounding grey matter. The lesion border is well defined and phenotypically stable by 7 DPI, but activated astrocytes continue to alter their expression patterns in spared grey and white matter regions for several weeks after injury. Finally, a potential immature precursor population, characterized by nestin expression and including cells that are BLBP+ and $GFAP^{neg}$, is short-lived and may be expanded only if targeted very early after injury. The ability to identify these different populations, including astrocyte precursors that may be induced to proliferate and develop into growth-promoting astrocytes, is a vital first step to improving endogenous repair after CNS injury via astrocyte-targeted manipulation.

Supplementary Material

Refer to Web version on PubMed Central for supplementary material.

Acknowledgments

The authors gratefully acknowledge the assistance of Patricia Walters and Feng Qin Yin with surgeries and animal care. We thank Jessica Alexander for critical review of the manuscript. Six and 24 HPI tissue was cut by Luke George Foley Smith. Confocal fluorescent images were collected at the OSU CMIF. This work was funded by R01 NS043246 and P30-NS045748.

This work was supported by R01 NS043246 and P30-NS045748

Literature Cited

Abe Y, Yamamoto T, Sugiyama Y, Watanabe T, Saito N, Kayama H, Kumagai T. Apoptotic cells associated with Wallerian degeneration after experimental spinal cord injury: A possible mechanism of oligodendoglial death. J Neurotrauma. 1999; 16:945–952. [PubMed: 10547103]

Anthony TE, Mason HA, Gridley T, Fishell G, Heintz N. Brain lipid-binding protein is a direct target of Notch signaling in radial glial cells. Genes Dev. 2005; 19:1028–1033. [PubMed: 15879553]

Barry D, McDermott K. Differentiation of radial glia from radial precursor cells and transformation into astrocytes in the developing rat spinal cord. GLIA. 2005; 50:187–197. [PubMed: 15682427]

Basso DM, Beattie MS, Bresnahan JC. Graded histological and locomotor outcomes after spinal cord contusion using the NYU weight-drop device versus transection. Exp Neurol. 1996; 139:244–256. [PubMed: 8654527]

Beck T, Lutz B, Theole U, Wree A. Assessing chronic brain damage by quantification of regional volumes in postischemic rat brains. Brain Res. 1993; 605:280–286. [PubMed: 8481778]

Buffo A, Rite I, Tripathi P, Lepier A, Colak D, Horn AP, Mori T, Gotz M. Origin and progeny of reactive gliosis: A source of multipotent cells in the injured brain. Proc Natl Acad Sci U S A. 2008; 105:3581–3586. [PubMed: 18299565]

Bullon MM, Alvarez-Gago T, Fernandez-Ruiz B, Aguirre C. Glial fibrillary acidic protein (GFAP) in spinal cord of postnatal rat: An immunoperoxidase study in semithin sections. Brain Res. 1984; 20:79–83. [PubMed: 6386101]

Burns KA, Murphy B, Danzer SC, Kuan CY. Developmental and post-injury cortical gliogenesis: A Genetic fate-mapping study with Nestin-CreER mice. GLIA. 2008; 57:1115–1129. [PubMed: 19115384]

Buss A, Schwab ME. Sequential loss of myelin proteins during Wallerian degeneriation in the spinal cord. GLIA. 2003; 42:424–432. [PubMed: 12730963]

Clarke SR, Shetty AK, Bradley JL, Turner DA. Reactive astrocytes express the embryonic intermediate neurofilament nestin. Neuroreport. 1994; 5:1885–1888. [PubMed: 7841369]

Costa S, Planchenault T, Charriere-Bertrand C, Mouchel Y, Fages C, Juliano S, Lefrancois T, Barlovatz-Meimon G, Tardy M. Astroglial permissivity for neuritic outgrowth in neuron-astrocyte cocultures depends on regulation of laminin bioavailability. GLIA. 2002; 37:105–113. [PubMed: 11754209]

De Leon M, Welcher AA, Nahin RH, Liu Y, Ruda MA, Shooter EM, Molina CA. Fatty acid binding protein is induced in neurons of the dorsal root ganglia after peripheral nerve injury. J Neurosci Res. 1996; 44:283–292. [PubMed: 8723767]

do Carmo Cunha CJ, de Freitas Azevedo LB, de Luca BA, de Andrade MS, Gomide VC, Chadi G. Responses of reactive astrocytes containing S100beta protein and fibroblast growth factor-2 in the border and in the adjacent preserved tissue after a contusion injury of the spinal cord in rats: implications for wound repair and neuroregeneration. Wound Repair Regen. 2007; 15:134–146. [PubMed: 17244329]

Eng LF, Vanderhaegan JJ, Bignami A, Gerstl B. An acidic protein isolated from fibrous astrocytes. Brain Res. 1971; 28:351–354. [PubMed: 5113526]

Faulkner JR, Herrmann JE, Woo MJ, Tansey KE, Doan NB, Sofroniew MV. Reactive astrocytes protect tissue and preserve function after spinal cord injury. J Neurosci. 2004; 24:2143–2155. [PubMed: 14999065]

Feng L, Hatten ME, Heintz N. Brain lipid-binding protein (BLBP): A novel signaling system in the developing mammalian CNS. Neuron. 1994; 12:895–908. [PubMed: 8161459]

Figueroa, JD.; Bu, L.; Serrano, M.; Miranda, JD.; De Leon, MA. Novel roles of fatty acid binding protein 5 in spinal cord injury. Poster presentation at the American Society for Neurochemistry conference; Charleston, SC. 2009.

Frisen J, Haegerstrand A, Risling M, Fried K, Johansson CB, Hammarberg H, Elde R, Hokfelt T, Cullheim S. Spinal axons in central nervous system scar tissue are closely related to laminin-immunoreactive astrocytes. Neuroscience. 1995a; 65:293–304. [PubMed: 7753403]

Frisen J, Johansson CB, Torok C, Risling M, Lendahl U. Rapid, widespread, and longlasting induction of nestin contributes to the generation of glial scar tissue after CNS injury. J Cell Biol. 1995b; 131:453–464. [PubMed: 7593171]

Guillery RW. On counting and counting errors. J Comp Neurol. 2002; 447:1–7. [PubMed: 11967890]

Haunerland NH, Spener F. Fatty acid binding proteins—insights from genetic manipulations. Prog Lipid Res. 2004; 43:328–349. [PubMed: 15234551]

Herrmann JE, Imura T, Song B, Qi J, Ao Y, Nguyen TK, Korsak RA, Takeda K, Akira S, Sofroniew MV. STAT3 is a critical regulator of astrogliosis and scar formation after spinal cord injury. J Neurosci. 2008; 28:7231–7243. [PubMed: 18614693]

Hochstim C, Deneen B, Lucasewicz A, Zhou Q, Anderson DJ. Identification of positionally distinct astrocyte subtypes whose identities are specified by a hemeodomain code. Cell. 2008; 133:510–522. [PubMed: 18455991]

Horky LL, Galimi F, Gage FH, Horner PJ. Fate of endogenous stem/progenitor cells following spinal cord injury. J Comp Neurol. 2006; 498:525–538. [PubMed: 16874803]

Ikeda O, Murakami M, Ino H, Yamazaki M, Nemoto T, Koda M, Nakayama C, Moriya H. Acute up-regulation of brain-derived neurotrophic factor expression resulting from experimentally induced injury in the rat spinal cord. Acta Neuropathol. 2001; 102:239–245. [PubMed: 11585248]

Inman D, Guth L, Steward O. Genetic influences on secondary degeneration and wound healing following spinal cord injury in various strains of mice. J Comp Neurol. 2003; 451:225–235. [PubMed: 12210135]

Ishii K, Nakamura M, Dai J, Finn TP, Okano H, Toyama Y, Bregman BS. Neutralization of ciliary neurotrophic factor reduces astrocyte production from transplanted neural stem cells and promotes regeneration of corticospinal tract fibers in spinal cord injury. J Neurosci Res. 2006; 84:1669–1681. [PubMed: 17044031]

Jakeman LB, Guan Z, Wei P, Ponnappan R, Dzwonczyk R, Popovich PG, Stokes BT. Traumatic spinal cord injury produced by controlled contusion in mouse. J Neurotrauma. 2000; 17:299–319. [PubMed: 10776914]

Johansson CB, Momma S, Clarke DL, Risling M, Lendahl U, Frisen J. Identification of a neural stem cell in the adult mammalian central nervous system. Cell. 1999; 96:25–34. [PubMed: 9989494]

Kempermann G, Gage FH. Neurogenesis in the adult hippocampus. Novaris Found Symp. 2000; 231:220–235.

Kerr BJ, Patterson PH. Potent pro-inflammatory actions of leukemia inhibitory factor in the spinal cord of the adultl mouse. Exp Neurol. 2004; 188:391–407. [PubMed: 15246839]

Kigerl KA, McGaughy VM, Popovich PG. Comparative analysis of lesion development and intraspinal inflammation in four strains of mice following spinal contusion injury. J Comp Neurol. 2006; 494:578–594. [PubMed: 16374800]

Kleeberger W, Bova GS, Nielsen ME, Herawi M, Chuang AY, Epstein JI, Berman DM. Roles for the stem cell associated intermediate filament Nestin in prostate cancer migration and metastasis. Cancer Res. 2007; 67:9199–9206. [PubMed: 17909025]

Krenz NR, Weaver LC. Nerve growth factor in glia and inflammatory cells of the injured rat spinal cord. J Neurochem. 2000; 74:730–739. [PubMed: 10646525]

Kuhn PL, Wrathall JR. A mouse model of graded contusive spinal cord injury. J Neurotrauma. 1998; 15:125–140. [PubMed: 9512088]

Lee MY, Kim CJ, Shin SL, Moon SH, Chun MH. Increased ciliary neurotrophic factor expression in reactive astrocytes following spinal cord injury in the rat. Neurosci Lett. 1998; 255:79–82. [PubMed: 9835219]

Lennington JB, Yang Z, Conover JC. Neural stem cells and the regulation of adult neurogenesis. Reprod Biol Endocrinol. 2003; 1:99. [PubMed: 14614786]

Liberto CM, Albrecht PJ, Herx LM, Yong VW, Levison SW. Pro-regenerative properties of cytokine-activated astrocytes. J Neurochem. 2004; 89:1092–1100. [PubMed: 15147501]

Liuzzi FJ, Lasek RJ. Astrocytes block axonal regeneration in mammals by activating the physiological stop pathway. Science. 1987; 237:642–645. [PubMed: 3603044]

Lytle JM, Chittajallu R, Wrathall JR, Gallo V. NG2 cell response in the CNP-EGFP mouse after contusive spinal cord injury. GLIA. 2009; 57:270–285. [PubMed: 18756526]

Lytle JM, Vicini S, Wrathall JR. Phenotype changes in NG2+ cells after spinal cord injury. J Neurotrauma. 2006; 23:1726–1738. [PubMed: 17184184]

Lytle JM, Wrathall JR. Glial cell loss, proliferation and replacement in the contused murine spinal cord. Eur J Neurosci. 2007; 25:1711–1724. [PubMed: 17432960]

Ma M, Basso DM, Walters P, Stokes BT, Jakeman LB. Behavioral and histological outcome following graded contusion injury in C57Bl/6 mice. Exp Neurol. 2001; 169:239–254. [PubMed: 11358439]

Ma M, Wei P, Wei T, Ransohoff RM, Jakeman LB. Enhanced axonal growth into a spinal cord contusion injury site in a strain of mouse (129X1/SvJ) with a diminished inflammatory response. J Comp Neurol. 2004; 474:469–486. [PubMed: 15174067]

McTigue DM, Wei P, Stokes BT. Proliferation of NG2-Positive Cells and Altered Oligodendrocyte Numbers in the Contused Rat Spinal Cord. J Neurosci. 2001; 21:3392–3400. [PubMed: 11331369]

Meletis K, Barnabe-Heider F, Carlen M, Evergren E, Tomilin N, Shupliakov O, Frisen J. Spinal cord injury reveals multilineage differentiation of ependymal cells. PLoS Biol. 2008; 6:e182. [PubMed: 18651793]

Mothe AJ, Tator CH. Proliferation, migration, and differentiation of endogenous ependymal region stem/progenitor cells following minimal spinal cord injury in the adult rat. Neuroscience. 2005; 131:177–187. [PubMed: 15680701]

Mothe AJ, Tator CH. Transplanted neural stem/progenitor cells generate myelinating oligodendrocytes and Schwann cells in spinal cord demyelination and dysmyelination. Exp Neurol. 2008; 213:176–190. [PubMed: 18586031]

Nakashima S, Matsuyama Y, Yu Y, Katayama Y, Ito Z, Ishiguro N. Expression of GDNF in spinal cord injury and its repression by ONO-1714. Neuroreport. 2005; 16:17–20. [PubMed: 15618882]

Namiki J, Tator CH. Cell proliferation and nestin expression in the ependyma of the adult rat spinal cord after injury. J Neuropathol Exp Neurol. 1999; 58:489–498. [PubMed: 10331437]

Okada S, Nakamura M, Katoh H, Miyao T, Shimazaki T, Ishii K, Yamane J, Yoshimura A, Iwamoto Y, Toyama Y, Okano H. Conditional ablation of Stat3 or Socs3 discloses a dual role for reactive astrocytes after spinal cord injury. Nat Med. 2006; 12:829–834. [PubMed: 16783372]

Panteri R, Mey J, Zhelyaznik N, D'Altocolle A, Del Fa A, Gangitano C, Marino R, Lorenzetto E, Buffelli M, Keller F. Reelin is transienty expressed in the peripheral nerve during development and is upregulated following nerve crush. Mol Cell Neurosci. 2006; 32:133–142. [PubMed: 16697663]

Pulido JS, Sugaya I, Comstock J, Sugaya K. Reelin is upregulated following ocular tissue injury. Graefes Arch Clin Exp Opthamol. 2007; 245:889–893.

Rehermann MI, Marichal N, Russo RE, Trujillo-Cenoz O. Neural reconnection in the transected spinal cord of the freshwater turtle *Trachemys dorbignyi*. J Comp Neurol. 2009; 515:197–214. [PubMed: 19418545]

Reier, PJ.; Stensaas, LJ.; Guth, L. The astrocytic scar as an impediment to regeneration in the nervous system. In: Kao, CC.; Bunge, RP.; Reier, PJ., editors. Spinal cord reconstruction. Raven Press; New York: 1983. p. 163-195.

Renault-Mihara F, Okada S, Shibata S, Nakamura M, Toyama Y, Okano H. Spinal cord injury: Emerging beneficial role of astrocytes' migration. Int J Biochem Cell Biol. 2008; 40:1649–1653. [PubMed: 18434236]

Rolls A, Shechter R, London A, Segev Y, Jacob-Hirsch J, Amariglio N, Rechavi G, Schwartz M. Two faces of chondroitin sulfate proteoglycan in spinal cord repair: a role in microglia/macrophage activation. PLoS Med. 2008; 5:e171. [PubMed: 18715114]

Rosen GD, Harry JD. Brain volume estimation from serial section measurements: A comparison of methodologies. J Neurosci Methods. 1990; 35:115–124. [PubMed: 2283883]

Rothstein JD, Dykes-Hoberg M, Pardo CA, Bristol LA, Jin L, Kuncl RW, Kanai Y, Hediger MA, Wang Y, Schielke JP, Welty DF. Knockout of glutamate transporters reveals a major role for astroglial transport in excitotoxicity and clearance of glutamate. Neuron. 1996; 16:675–686. [PubMed: 8785064]

Rudge JS, Silver J. Inhibition of neurite outgrowth on astroglial scars in vitro. J Neurosci. 1990; 10:3594–3603. [PubMed: 2230948]

Santos-Silva A, Fairless R, Frame MC, Montague P, Smith GM, Toft A, Riddell JS, Barnett SC. FGF/heparin differentially regulates Schwann cell and olfactory ensheathing cell interactions with astrocytes: A role in astrocytosis. J Neurosci. 2007; 27:7154–7167. [PubMed: 17611269]

Sellers DL, Maris DO, Horner PJ. Postinjury niches induces temporal shifts in progenitor fates to direct lesion repair after spinal cord injury. J Neurosci. 2009; 29:6722–6733. [PubMed: 19458241]

Schmid RS, Yokota Y, Anton ES. Generation and characterization of brain lipid-binding protein promoter-based transgenic mouse models for the study of radial glia. GLIA. 2006; 53:345–351. [PubMed: 16288463]

Shuman SL, Bresnahan JC, Beattie MS. Apoptosis of microglia and oligodendrocytes after spinal cord contusion in rats. J Neurosci Res. 1997; 50:798–808. [PubMed: 9418967]

Sroga JM, Jones TB, Kigerl KA, MCGaughy VM, Popovich PG. Rats and mice exhibit distinct inflammatory reactions after spinal cord injury. J Comp Neurol. 2003; 462:223–240. [PubMed: 12794745]

Tohyama T, Lee VM, Rorke LB, Marvin M, McKay RD, Trojanowski JQ. Nestin expression in embryonic human neuroepithelium and in human neuroepithelial tumor cells. Lab Invest. 1992; 66:303–313. [PubMed: 1538585]

Tom VJ, Doller CM, Malouf AT, Silver J. Astrocyte-associated fibronectin is critical for axonal regeneration in adult white matter. J Neurosci. 2004; 24:9282–9290. [PubMed: 15496664]

Tripathi R, McTigue DM. Prominent oligodendrocyte genesis along the border of spinal contusion lesions. GLIA. 2007; 55:698–711. [PubMed: 17330874]

Tripathi RB, McTigue DM. Chronically increased ciliary neurotrophic factor and fibroblast growth factor-2 expression after spinal contusion in rats. J Comp Neurol. 2008; 510:129–144. [PubMed: 18615534]

Vijayan VK, Lee YL, Eng LF. Increase in glial fibrillary acidic protein following neural trauma. Mol Chem Neuropathol. 1990; 13:107–118. [PubMed: 2095779]

Whetstone WD, Hsu JY, Eisenberg M, Werb Z, Noble-Haeusslein LJ. Blood-spinal cord barrier after spinal cord injury: relation to revascularization and wound healing. J Neurosci Res. 2003; 74:227–239. [PubMed: 14515352]

White RE, Jakeman LB. Don't fence me in: harnessing the beneficial roles of astrocytes for spinal cord repair. Restor Neurol Neurosci. 2008; 26:197–214. [PubMed: 18820411]

Widenfalk J, Lundstromer K, Jubran M, Brene S, Olson L. Neurotrophic factors and receptors in the immature and adult spinal cord after mechanical injury or kainic acid. J Neurosci. 2001; 21:3457–3475. [PubMed: 11331375]

Wu D, Shibuya S, Miyamoto O, Itano T, Yamamoto T. Increase of NG2-positive cells associated with radial glia following traumatic spinal cord injury in adult rats. J Neurocytol. 2005; 34:459–469. [PubMed: 16902766]

Xu Y, Kitada M, Yamaguchi M, Dezawa M, Ide C. Increase in bFGF-responsive neural progenitor population following contusion injury of the adult rodent spinal cord. Neurosci Lett. 2006; 397:174–179. [PubMed: 16406666]

Yamamoto S, Yamamoto N, Kitamura T, Nakamura K, Nakafuku M. Proliferation of parenchymal neural progenitors in response to injury in the adult rat spinal cord. Exp Neurol. 2001; 172:115–127. [PubMed: 11681845]

Yang H, Lu P, McKay HM, Bernot T, Keirstead H, Steward O, Gage FH, Edgerton VR, Tuszynski MH. Endogenous neurogenesis replaces oligodendrocytes and astrocytes after primate spinal cord injury. J Neurosci. 2006; 26:2157–2166. [PubMed: 16495442]

Zai LJ, Wrathall JR. Cell proliferation and replacement following contusive spinal cord injury. GLIA. 2005; 50:247–257. [PubMed: 15739189]

Zhang Z, Fujiki M, Guth L, Steward O. Genetic influences on cellular reactions to spinal cord injury: A wound-healing response present in normal mice is impaired in mice carrying a mutation (Wld^S) that causes delayed Wallerian degeneration. J Comp Neurol. 1996; 371:485–495. [PubMed: 8842901]

Zhu X, Bergles DE, Nishiyama A. NG2 cells generate both oligodendrocytes and gray matter astrocytes. Development. 2008a; 135:145–57. [PubMed: 18045844]

Zhu X, Hill RA, Nishiyama A. NG2 cells generate oligodendrocytes and gray matter astrocytes in the spinal cord. Neuron Glia Biol. 2008b; 13:1–8.

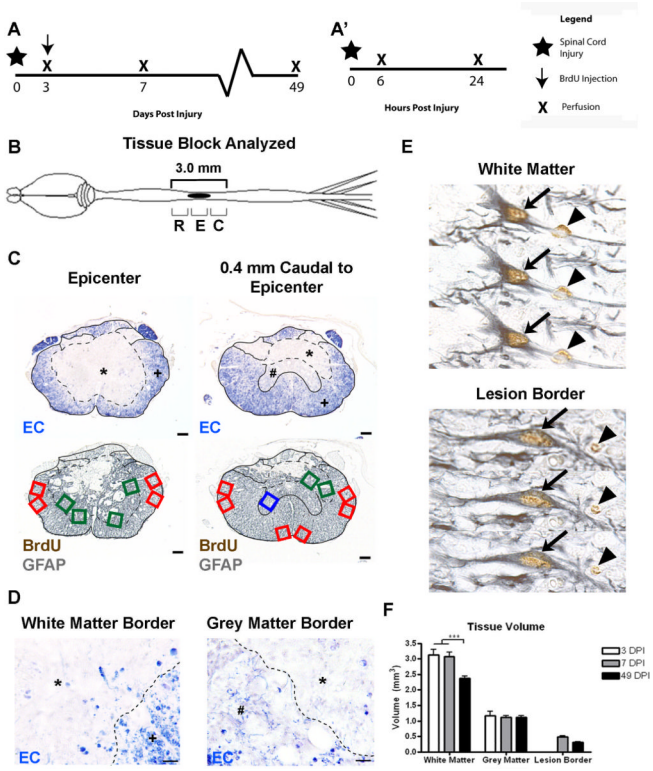

Figure 1.

BrdU+ and BrdU+/GFAP+ cell counting paradigm. (A) Time course of the two experiments as described in the methods, showing the BrdU administration paradigm used for BrdU+/GFAP+ cell counting (A) and acute marker expression analysis (A'). (B) Schematic drawing of the CNS with a midthoracic SCI, indicated by the solid black oval. Sections were examined at 200 μm intervals from 1.4 mm rostral to 1.4 mm caudal from the lesion epicenter, and these regions were further divided into Rostral-R, Epicenter-E, and Caudal-C levels for quantitative analyses. (C) Examples of 2 pairs of transverse spinal cord sections are shown from the epicenter (left) and 0.4 mm caudal to the epicenter (right). EC staining was used to identify the distribution of the lesion edge (dashed line) and spared grey matter and spared white matter. Sample fields were counted in adjacent tissue sections stained with BrdU and GFAP antisera. Green boxes indicate lesion border areas, red boxes indicate spared white matter, and blue boxes indicate spared grey matter. * indicates the lesion, # depicts spared grey matter, and + is spared white matter. (D) High-magnification images of white matter (left) and grey matter (right) borders, with the lesion border depicted by a dashed line. (E) Examples of double-labeled BrdU+/GFAP+ cells in spared white matter (top) and lesion border (bottom), through three planes of focus. Single labeled BrdU+ cells are identified by an arrowhead, while double labeled cells are indicated by an arrow. (F) Quantification of changes in total tissue volume in different regions over time. Scale = 100 μm (C), 10 μm (D).

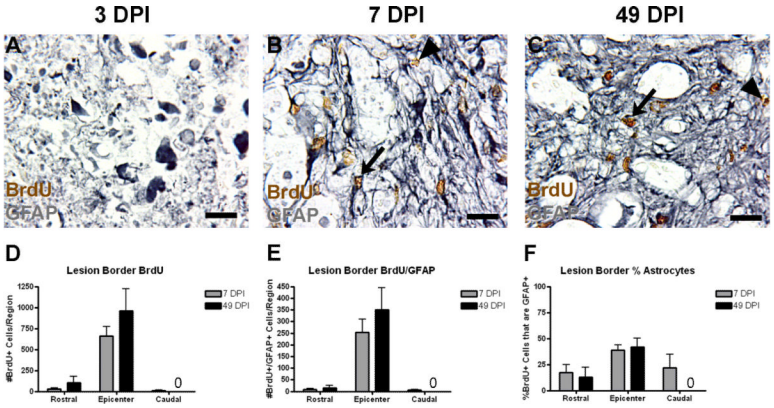

Figure 2.

Early proliferating cells accumulate at the lesion border by 7 DPI. (A–C) Representative images of lesion border regions at the injury epicenter at 3 (A), 7 (B), and 49 DPI. Examples of single and double-labeled cells are indicated by arrowheads and arrows, respectively. (D–F) Quantification of the number of BrdU+ cells (D), number of BrdU+/GFAP+ cells (E), and the percentage of BrdU+ cells also expressing GFAP (F) at 7 and 49 DPI. Cell counts were not performed for this region at 3 DPI because the region is not yet defined. “0” in graphs designate no cells in the indicated regions. Scale = 10 μm.

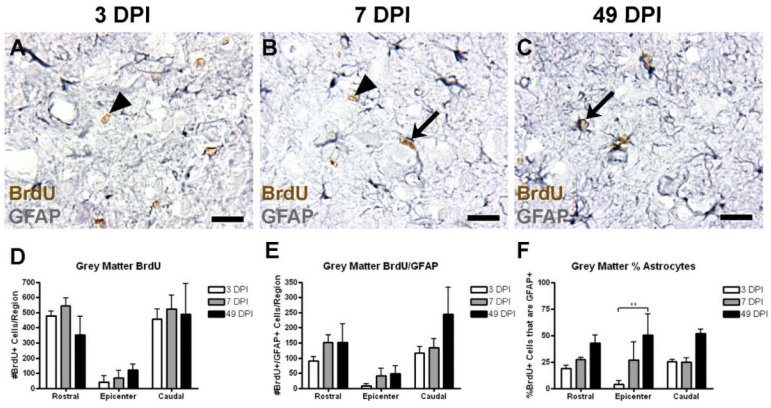

Figure 3.

The number of BrdU+ and BrdU+/GFAP+ cells is unchanged in spared grey matter after SCI. (A–C) Representative images of spared grey matter 1.0 mm caudal from the injury epicenter at 3 (A), 7 (B), and 49 DPI (C). Examples of single and double labeled cells are indicated with arrowheads and arrows, respectively. (D–F) Quantification of the number of BrdU+ cells (D), number of BrdU+/GFAP+ cells (E), and the percentage of BrdU+ cells also expressing GFAP (F) in spared grey matter at 3, 7, and 49 DPI. Scale = 10 μm. **$p < 0.01$ (% of astrocytes in the epicenter region at 3 vs. 39 DPI).

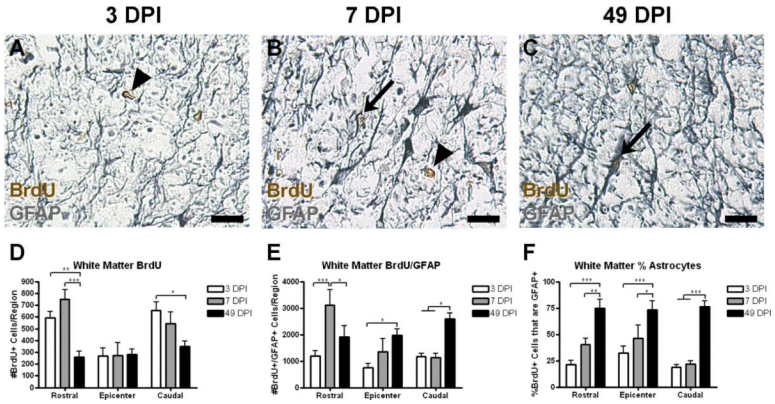

Figure 4.

In spared white matter, the number of BrdU+ cells decreases over time while the number of and percentage of BrdU+/GFAP+ cells increases. (A–C) Representative images of spared grey matter 1.0 mm caudal from the injury epicenter at 3 (A), 7 (B), and 49 DPI (C), with examples of single and double-labeled cells indicated with arrowheads and arrows, respectively. (D–F) Quantification of the number of BrdU+ cells (D), number of BrdU+/GFAP+ cells (E), and the percentage of BrdU+ cells also expressing GFAP (F) in spared white matter. Scale = 10 μm. *$p < 0.05$ (BrdU+ cells in the caudal region 3 vs. 49 DPI; BrdU+/GFAP+ cells in the rostral region 7 vs. 49 DPI; BrdU+/GFAP+ cells in the epicenter region 3 vs. 49 DPI; BrdU+/GFAP+ cells in the caudal region 3 and 7 vs. 49 DPI; % astrocytes in the epicenter region 7 vs. 49 DPI), **$p < 0.01$ (BrdU+ cells in the rostral region 3 vs. 49 DPI; % astrocytes in the rostral region 7 vs. 49 DPI), ***$p < 0.001$ (BrdU+ cells in the rostral region 7 vs. 49 DPI; BrdU+/GFAP+ cells in the rostral region 3 vs. 7 DPI; % astrocytes in all regions 3 vs. 49 DPI).

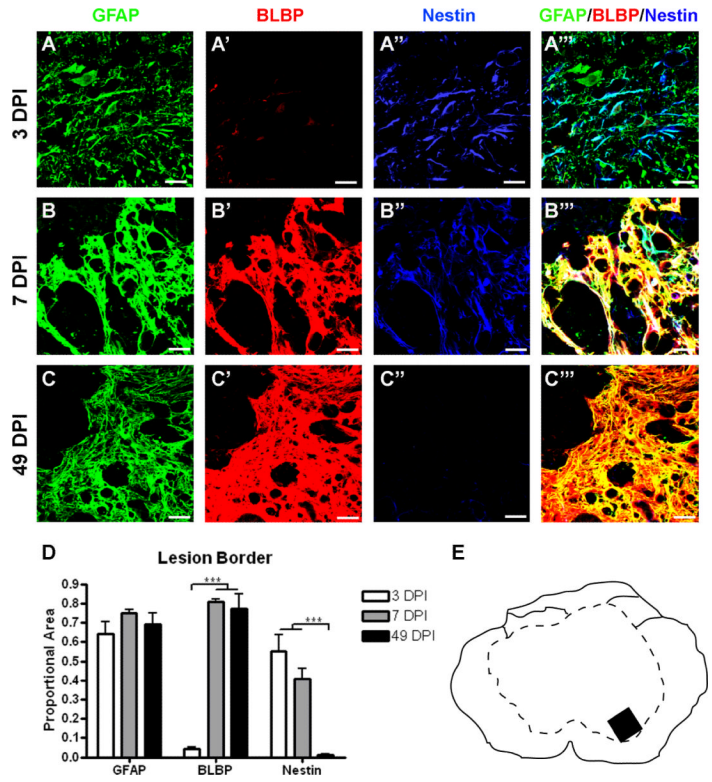

Figure 5.

Nestin expression increases transiently after injury in the lesion border, while BLBP levels rise later and stay high chronically. (A–C) Representative confocal images of GFAP (green), BLBP (red), and nestin (blue) expression and merged images of three markers (right) at 3 DPI (A–A'''), 7 DPI (B–B''') and 49 DPI (C–C'''). (D) Quantification of the proportion of merged staining area represented by GFAP, BLBP, and nestin expression levels over time. Scale = 20 μm. (E) Schematic depicting region shown in confocal images. ***$p < 0.001$ (BLBP 3 vs. 7 and 49 DPI; nestin 3 and 7 vs. 49 DPI).

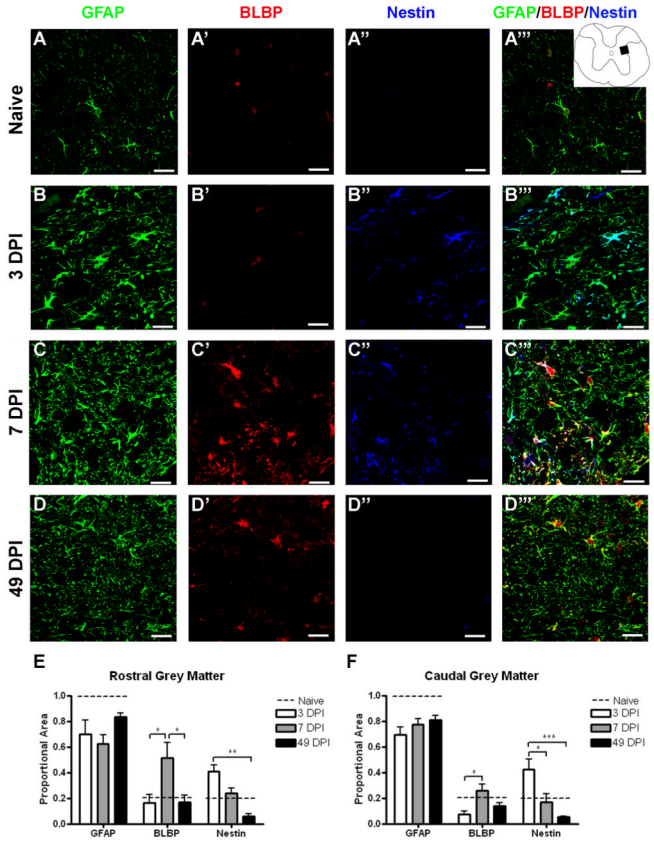

Figure 6.

BLBP and nestin expression transiently increase in spared grey matter. (A–D) Confocal images of GFAP (green), BLBP (red), and nestin (blue) in naïve tissue (A–A‴) and 1.0 mm caudal from the lesion epicenter at 3 (B–B‴), 7 (C–C‴) and 49 (D–D‴) DPI. Inset depicts region shown in confocal images. (E–F) Quantification of the proportion of merged staining area represented by GFAP, BLBP, and nestin immunoreactivity over time both rostral (E) and caudal (F) to the injury epicenter. The dashed line in each graph depicts the proportion of merged staining colocalized with each of the markers in naïve tissue specimens. Scale = 20 μm. *$p < 0.05$ (BLBP rostral 3 vs. 7 vs. 49 DPI; BLBP caudal 3 vs. 7 DPI; nestin caudal 3 vs. 7 DPI), **$p < 0.01$ (nestin rostral 3 vs. 49 DPI), ***$p < 0.001$ (nestin caudal 3 vs. 49 DPI).

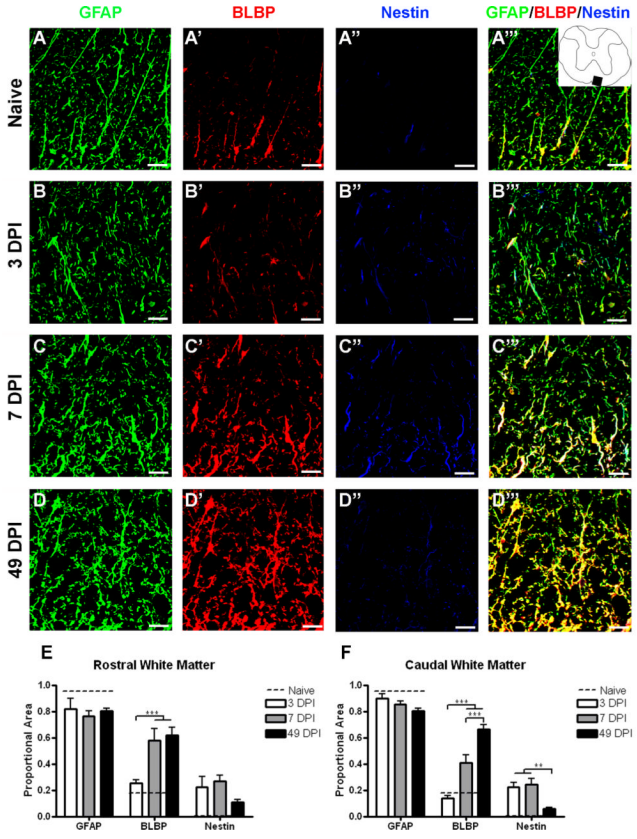

Figure 7.

BLBP expression is chronically upregulated in spared white matter, while nestin expression only transiently increases. (A–D) Confocal images of GFAP (green), BLBP (red), and nestin (blue) in naïve tissue (A–A‴) and 1.0 mm caudal from the lesion epicenter at 3 (B–B‴), 7 (C–C‴) and 49 (D–D‴) DPI. Inset depicts region shown in confocal images. (E–F) Quantification of the proportion of merged staining area represented by GFAP, BLBP, and nestin immunoreactivity over time both rostral (E) and caudal (F) to the injury epicenter. The dotted line in each graph depicts the proportion of merged staining colocalized with each of the markers in naïve tissue specimens. Scale = 20 μm. **$p < 0.01$ (nestin caudal 3 and 7 vs. 49 DPI), ***$p < 0.001$ (BLBP rostral 3 vs. 7 and 49 DPI; BLBP caudal 3 vs. 7 and 49 DPI; BLBP caudal 7 vs. 49 DPI).

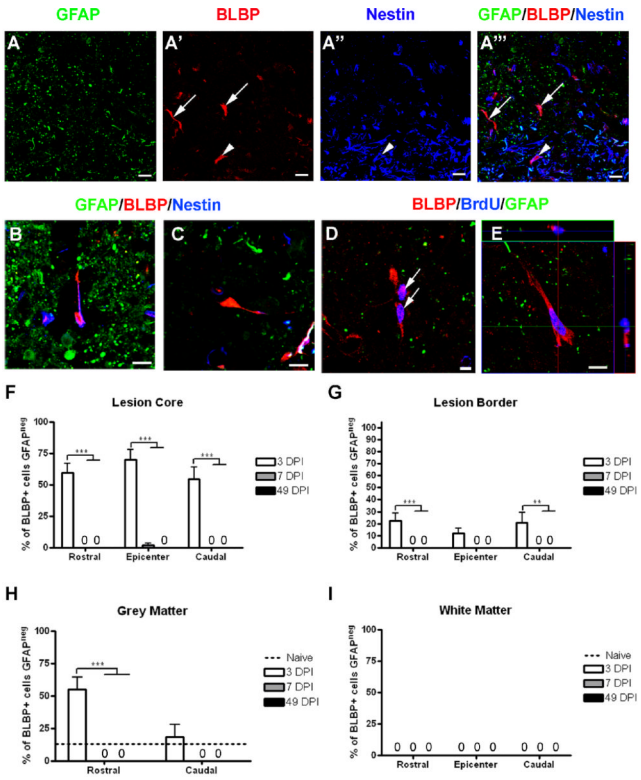

Figure 8.

BLBP+/GFAP^{neg} cells are present early after injury and exhibit a unique morphology. (A–A''') Confocal images of GFAP (green), BLBP (red), and nestin (blue) showing examples of BLBP+/GFAP^{neg} cells that do (arrowhead in A''', B) and do not (arrows in A''', C) express nestin. (D) Confocal image showing examples of BLBP+/GFAP^{neg} cells expressing BrdU (blue). (E) Confocal z-stack confirming double-labeling of BLBP and BrdU. (F–I) Quantification of the percentage of BLBP+ cells from the lesion core (F), lesion border (G), spared grey matter (H), and spared white matter (I) that did not express GFAP. Scale = 20 μm (A–A'''), 5 μm (B–E). **$p < 0.01$ (lesion border caudal 3 vs. 49 DPI), ***$p < 0.001$ (lesion core all regions 3 vs. 7 and 49 DPI; grey matter rostral 3 vs. 7 and 49 DPI).

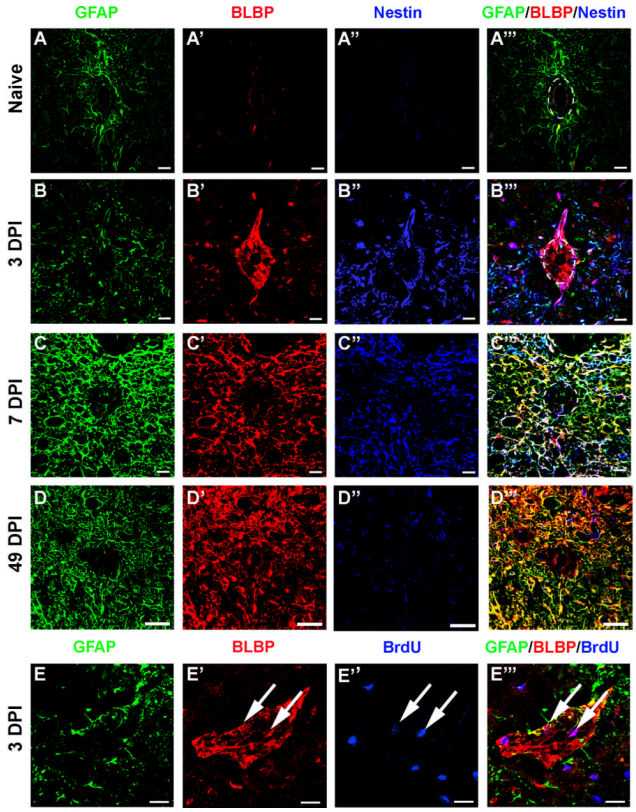

Figure 9.

BLBP expression is transiently increased in cells lining the central canal early after injury. (A–D) Confocal images showing GFAP (green), BLBP (red), and nestin (blue) expression in the naïve central canal at spinal level T9 (A–A‴) and in the central canal region caudal to the epicenter at 3 DPI (B–B‴), 7 DPI (C–C‴), and 49 DPI (D–D‴). (E) Example of a BrdU+ cells (blue) colabeled with BLBP (red) in the central canal at 3 DPI (arrows). Scale = 20 μm.

Table 1

Antibody Characterization

Antigen	Immunogen	Species	Mono- vs. Polyclonal	Manufacturer	Catalog and Lot #	Dilution Used
Brain Lipid Binding Protein (BLBP)	Recombinant whole mouse BLBP	Rabbit	Polyclonal	Millipore	Cat # AB9558	1:2000
Bromodeoxyuridine (BrdU)	BrdU	Rat	Monoclonal	AbD Serotec	Cat# MCA2060	1:100
Glial Fibrillary Acidic Protein (GFAP)	GFAP from cow spinal cord	Rabbit	Polyclonal	Dako	Cat# Z0334	1:5000 (SG); 1:1000 (FL)
Nestin	EKE DQR FPR SPE EDQ Q; EKE RQE SLK SPE DED QQ; EVE EGP ERE QHQ ESL RS	Chicken	Polyclonal	Aves Labs	Cat# NES	1:500